JOURNAL OF THE ROYAL SOCIETY OF NEW ZEALAND
2025, VOL. 55, NO. 4, 1051–1072
https://doi.org/10.1080/03036758.2024.2308015

Taylor & Francis
Taylor & Francis Group

RESEARCH ARTICLE

OPEN ACCESS Check for updates

A parametric analysis of a solar humidification/dehumidification desalination system using a bio-inspired cascade humidifier

Reza Enayatollahi[a], Timothy Anderson [b,c] and Roy Nates[d]

[a]Department of Engineering Technology, Toi Ohomai Institute of Technology, Tauranga, New Zealand; [b]School of Energy, Engineering and Infrastructure, Western Institute of Technology, New Plymouth, New Zealand; [c]School of Engineering and Computer Science, Victoria University of Wellington, Wellington, New Zealand; [d]School of Engineering, Computer and Mathematical Sciences, Auckland University of Technology, Auckland, New Zealand

ABSTRACT

Water scarcity is a significant challenge for a growing world's population, particularly in remote locations where solar energy is plentiful. Of the existing solutions, the Humidification-Dehumidification (HDH) desalination technique can work effectively with low-grade energy sources, such as solar. However, HDH desalination systems often have a low yield, leading to a focus on ever-more complex humidification systems. This work aims to examine the performance of a novel bioinspired humidifier as a low-cost and effective solution to increase the yield of small-scale HDH desalination systems. To this end, an HDH desalination system using a cascade humidifier was conceptually developed and parametrically modelled. It was shown that the evaporation rate in the humidifier could be increased by increasing both the air and water flow rates. It was also found that an evaporation rate of 0.91×10^{-3} kg/s could be achieved for an evaporation area of 0.36 m^2. Considering the entire desalination system, it was noted that increasing the water flow rate reduced the water temperature entering the humidifier and thus reduced production. Conversely, increasing the airflow rate enhanced the production rate. More importantly, it was shown that under appropriate conditions this novel desalination system can have a production of 10.2 litre/day/m^2.

ARTICLE HISTORY
Received 17 October 2023
Accepted 16 January 2024

HANDLING EDITOR
Alan Brent

KEYWORDS
Cascade humidifier; desalination; humidification-dehumidification; cross-flow interaction; solar

Nomenclature

A	Area (m^2)
Bd	Bodenstein number
c	Capacity ratio
C_B	Bond conductance (W/m.K)
c_p	Specific heat (J/kg.K)

CONTACT Reza Enayatollahi reza.enayatollahi@toiohomai.ac.nz

D	Diameter (m)
E	Effectiveness
F	Fin efficiency
F'	Efficiency factor
F_R	Heat removal factor
G	Radiation (W/m^2)
$\hbar$	Enthalpy (J/kg)
$\hbar_{fg}$	Latent heat of evaporation
h	Heat transfer coefficient (W/m^2.K)
H	Height (m)
j	Mass transfer coefficient (m/s)
k	Thermal conductivity (W/m.K)
L	Length (m)
Le	Lewis number
l	Thickness (m)
$\dot{m}$	Mass flow rate (kg/s)
N_{ev}	Evaporation number
NTU	Number of transmitted units
Nu	Nusselt number
P	Pressure (atm)
Pe	Peclet number
Pr	Prandtl number
$\dot{Q}$	Rate of heat transfer (W)
r	Radius (m)
R	Specific gas constant
Re	Reynolds number
Rh	Relative humidity
s	Angle of solar water collector from the horizon
Sc	Schmidt number
Sh	Sherwood number
S_τ	Tube pitch (m)
T	Temperature (K)
U	Overall heat transfer coefficient (W/m^2.K)
U'	Overall heat loss coefficient
$\dot{V}$	Volumetric Flow rate
w	Tube spacing (m)
W	Width (m)
We	Weber number
ε	Emissivity
λ	Mass diffusivity (m^2/s)
ρ	Density (kg/m^3)
σ	Stephan-Boltzmann constant (W/m^2.K^4)
π	The number Pi

Subscript

a	Air
abs	Absorbed
amb	Ambient
a-w	Air to water
c	Capacity ratio
ch	Characteristic
chn	Channel
col	Collector
cond	Condenser
conv	Convection
econ	Economiser

ev	Evaporation
f	Film
gl	Glass cover
hmd	Humidifier
i	Inner
in	Inlet
ins	Insulation
max	Maximum
min	Minimum
NTU	Number of transfer units
o	Outer
out	Outlet
p	Absorber plate
Pr	Perimeter
sat	Saturation
u	Useful
v	Vapour
w	Water
wd	Wind
τ	Tube

Introduction

Nearly three-quarters of the earth's surface is covered with water, but only 3% of this water is potable (Al-Juwayhel et al. 1997). That is to say, it contains 500 ppm or less of salt (Al-Enezi et al. 2006). By 2040 it has been suggested that approximately 50% of the world's population would be living in water-stressed regions (Luo et al. 2015; Shaikh and Ismail 2022). Therefore, a large number of investigations have been aimed at finding efficient and clean techniques for water treatment (Yuan and Zhang 2007; Srithar and Rajaseenivasan 2018; Lawal and Qasem 2020; Abu El-Maaty et al. 2023; Shamet et al. 2023), including desalination systems. Many current-generation desalination plants use fossil fuels to provide heat and electrical energy to the membrane technologies they frequently use (Giwa et al. 2016; Shaikh and Ismail 2022). However, these systems are often costly and not environmentally sustainable (Qtaishat and Banat 2013). Furthermore, the complexity and high energy requirements often make these systems inappropriate for small-scale water production in remote locations, where lack of access to potable water is most pronounced. Many of these remote locations are in regions considered to be barren, though coincidently they are often rich in solar energy. Hence, using solar energy to provide the required energy to desalinate non-potable water appears to be an obvious solution.

In this vein, the humidification/dehumidification (HDH) desalination technique has been receiving a significant degree of attention, primarily due to its low-temperature nature. The HDH technique mimics the natural rain cycle, and systems based on this approach potentially offer low cost and flexibility in their configuration (Narayan et al. 2010; Al-Sulaiman et al. 2015). Additionally, the advancement in harvesting solar thermal energy by water/air solar collectors (Morrison et al. 2004; Gill et al. 2012; Sabiha et al. 2015; Abokersh et al. 2017; Nowzari et al. 2021), has the potential to enhance the system's performance and reduce their capital and operating costs. However, much of the work undertaken on these systems is focused on larger-scale systems, that may be appropriate to remote locations. As an example, Yuan et al.

(2007) carried out an experimental study on a two-staged HDH system with closed air and water cycles. It was reported that with the thermal storage provided by the seawater tank, the system was able to operate 24 h a day with a production of 5.2 L/m^2/day in June and 2.7 L/day/m^2 in December in Xi'an, China. It was also concluded that for a fixed solar absorber area, production decreased with increasing water flow rate and that by proper utilisation of the latent heat, the process efficiency could increase.

In 2014 Zamen et al. (2014) performed an experimental investigation on a two-stage solar HDH system, in an attempt to increase performance and productivity. It was reported that a two-stage HDH desalination unit led to a 20% increase in production compared to a similar single-stage unit. The maximum productivity of potable water production during summertime with 80 m^2 of solar absorber area was reported to be 7.25 L/day/m^2. Similarly, Fouda et al. (2018), conducted a parametric study on the performance of three HDH desalination systems: a single-stage, a double-stage system, and a multistage system, under both closed and open modes. The highest production reported was 35 L/day/m^2 from the multistage system. It was also found that an open mode of operation performed better under warm and humid conditions, while for drier ambient air, a closed system would perform better.

One of the primary challenges of HDH systems is maximising the amount of water that is captured in the humidification process. Hence, humidifier design has been a significant area of attention for these systems. In the HDH system of Hallaj et al. (1998) water was sprayed over the humidifier after being pre-heated by the moist air from the humidifier and passing through a flat plate solar collector. The water spray in the humidifier heated and humidified cold air coming from the condenser, which then returned to the condenser. It was reported that the production of this system increased with increasing water flowrates. However, it was also observed that there existed an optimum value, beyond which production decreased.

In a similar attempt to improve the humidification spray cooling packed bed towers are often used in HDH systems as they provide large humidification areas and contact time. Tan et al. (2023) performed a developed 2D model of a direct contact crossflow packed bed condenser and experimentally validated the result of the model, and an effectiveness of 93% to 96% is reported based on the condensation rate. Soomro et al. (2022) theoretically and experimentally investigated the effect of different packing materials, and reported a maximum production of 0.64 L/hour. Similarly Zarei et al. (2022) studied an HDH desalination system with direct contact packed towers, and reported production of 300 L/day. Finally, Abdel Dayem et al. (2022) carried out a psychrometric analysis on the performance of a new packing material in an attempt to enhance the evaporation process in the humidifier. They reported that during a hot summer day (60°C) a production of 28 L/day/m^2 from a solar collector (parabolic dish) could be achieved.

Although the HDH desalination systems with spray cooling towers and packed materials have high production rates and efficiency (Luberti and Capocelli 2023), this is often tied to a significant pressure drop across the packing material and spray nozzles (Narayan et al. 2010). Overcoming this issue necessitates the use of delicate high-pressure pumps and fans. As a case in point, in the study by Abdel Dayem (2022), the pump and fan power were 0.66 and 0.25 kW while the total heat energy input was only 1.5 kW. As such,

this work aimed to conceptually develop and analyse an HDH desalination system with a humidifier that would lend itself to small scale implementation.

System overview

As noted previously, the HDH desalination system mimics the rain cycle observed in nature. To achieve this, it utilises several typical components: a solar water heater, a condenser and economiser, and perhaps most importantly a humidifier, arranged as shown in Figure 1.

Simply speaking, the cycle utilises two working fluids, air and water. On the water side of the cycle, cold saline water is drawn from its source and pumped through a condenser, where it removes heat from the air in the cycle. Subsequently, it passes through an economiser where it is further heated by the waste brine stream of the cycle. This, now preheated, saline water then enters a solar water heater, where it absorbs heat from the incident solar radiation, thus exiting a significantly higher temperature than it entered with. This hot saline water then enters the humidifier, where it is mixed with the cool ambient air thus humidifying it. Finally, any water that is unable to humidify the air exits as a concentrated warm waste brine stream to the economiser where it preheats the incoming cold saline stream.

On the air side of the cycle, air is drawn from the ambient surroundings and mixed with the hot saline water in the humidifier. It exits the humidifier and enters the condenser, where it gives up its heat to the cold inlet water, and in doing so is stripped of some of its water content (assuming the saline water's temperature is below the dew point temperature of the air). This water is then captured in a storage vessel whilst the air is allowed to return to the ambient surroundings.

From the literature, it was apparent that the humidification process plays a key role in determining the yield from an HDH system. Now, whilst highly effective, spray and

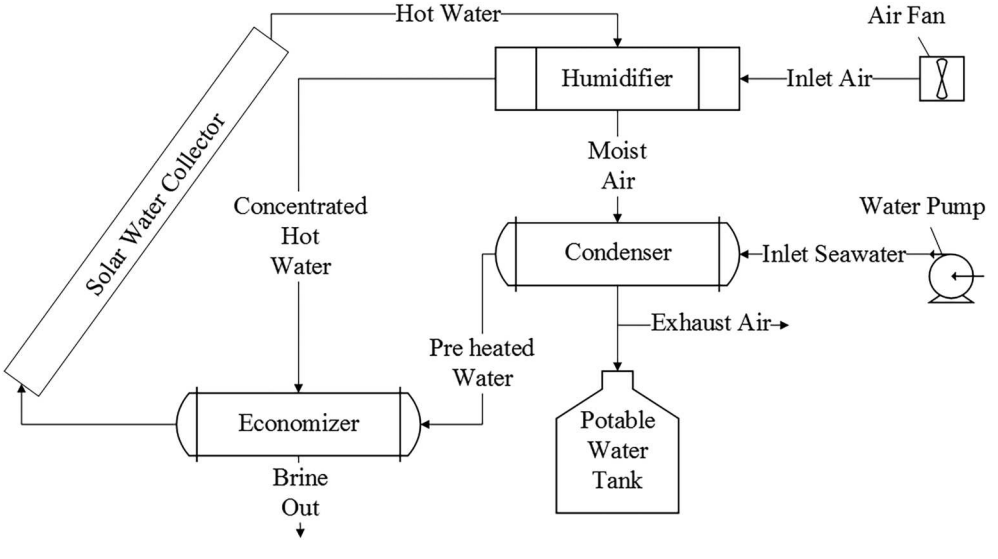

Figure 1. Proposed solar heated HDH desalination unit.

packed bed humidifiers, higher energies are required to pump air and water through the nozzles and porosities of the packing materials, which can only get worse due to fouling. This would increase the maintenance and operating costs and therefore these two types of humidifiers would likely be unsuitable for implementation into a small-scale HDH system. Hence, to address the issue of humidification, this work chose to draw inspiration from nature, and the transfer processes that occur in free-falling waterfalls for the humidifier design.

As anyone who has stood behind a waterfall will appreciate, the air passing through it is particularly humid. This is because as the air flows through the falling sheets of water it tends to atomise the water which then mixes with the air (Enayatollahi et al. 2017, 2017b). It was this observation that led to the proposal for a novel humidifier, consisting of a series of 'waterfalls' being proposed, as shown in Figure 2.

In this humidifier, two main types of interaction exist; counter-current and crossflow. The counter-current interaction is the same as that in a rectangular duct, where water flows along the base and air flows above the water surface. However, the crossflow interaction is more complicated, due to the presence of multiple flow regimes and interactions, as described in (Enayatollahi et al. 2017b).

System model

Quite obviously, the performance of a solar HDH desalination system will be closely tied to the meteorological conditions in which it operates. Hence for this study, it was decided to examine the yield on a 'typical' summer day where the solar radiation is 1000 W/m^2, the wind speed is 5 m/s, the atmospheric pressure is 1 atm, the average saline water temperature (for desalination) is 15°C, the ambient air temperature is 20°C and the relative humidity is 50%. To achieve this a parametric model was developed using Engineering Equation Solver (EES) (Klein 2016). In implementing the model, the fluid properties in EES were used to solve the parametric equations used to describe the individual components in the cycle. Given the nature of the equations, an iterative approach was required to reach a solution for the system, as illustrated in Figure 3. In saying this, the model estimates the temperatures of air and water leaving the humidifier, and examines the difference between the estimates of the exiting air and water temperature and the

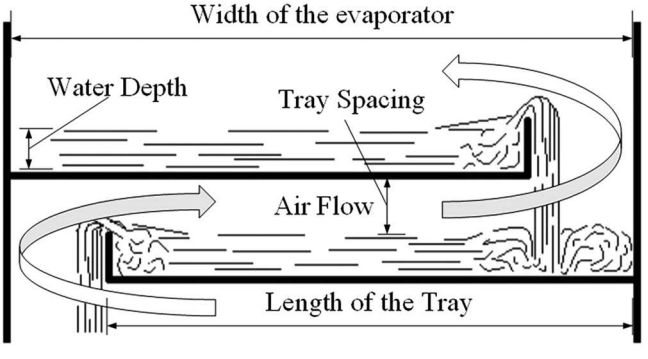

Figure 2. Schematic representation of a section of the novel cascading humidifier.

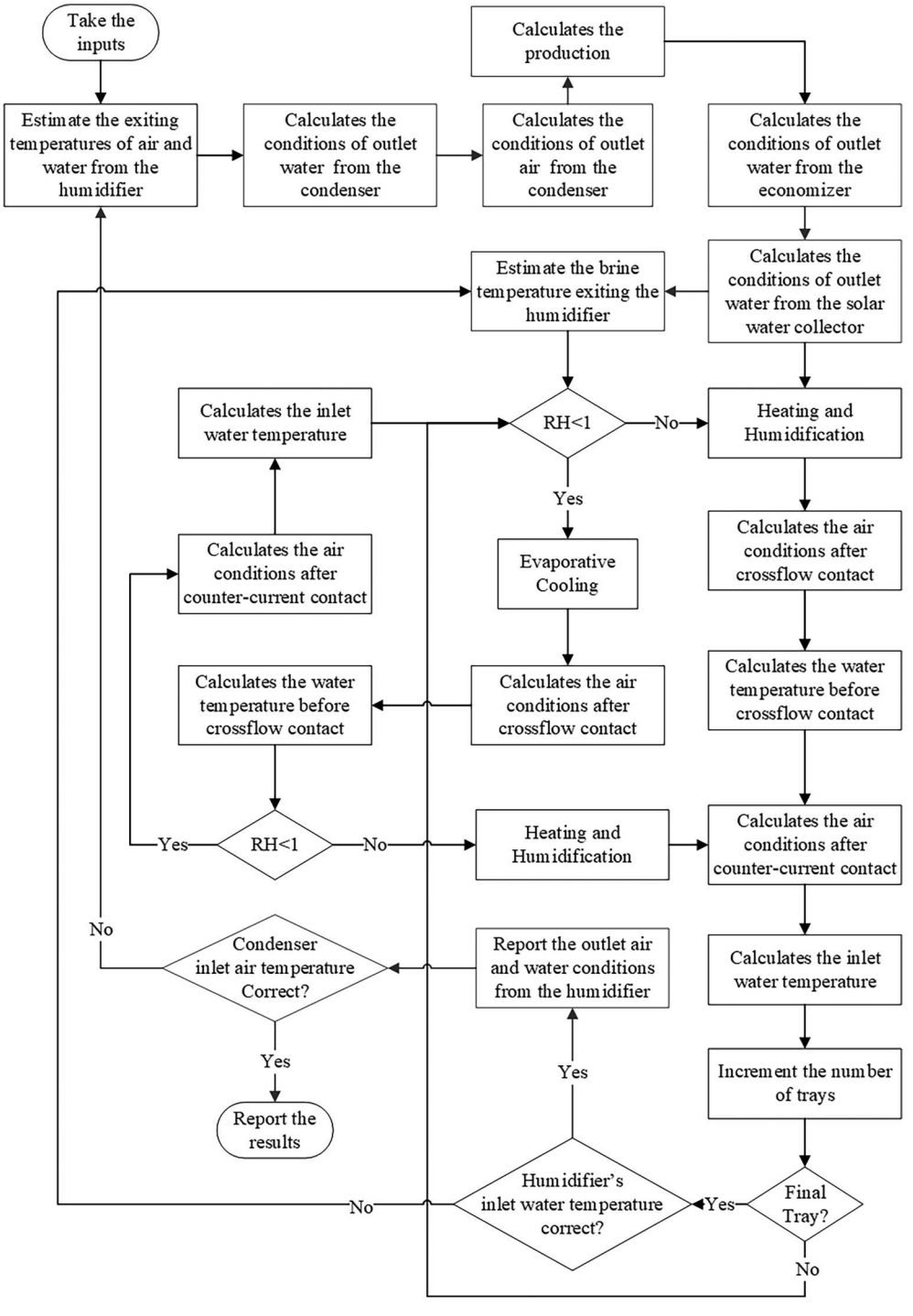

Figure 3. The flow chart diagram of the algorithm used for the model.

calculated values after the iteration. It was assumed that a solution was achieved when the difference between these was less than 0.01°C.

Solar water heater

Perhaps second in importance to the humidifier is the solar collector, that captures the thermal energy required to drive the HDH process. For this analysis, it was assumed that a small-scale HDH system would use a typical flat plate solar collector, as they have been used extensively in other HDH and desalination systems (Elminshawy et al. 2015). Therefore, a simple standard double-glazed flat plate solar water collector was modelled as the heat source for the HDH system. Hence, the Hottel-Whillier equations (Equations (1)–(12)) (Duffie and Beckman 1980) were used in order to mathematically model the collector.

As such, the outlet water temperature from the collector can be calculated from Equation (1).

$$T_{w,out,col} = T_{w,in,col} + \frac{\dot{Q}_{u,\,col}}{\dot{m}_{w,in,col} c_{pw,col}} \tag{1}$$

Where the rate of useful energy gained by water, associated with Equation (1), can be determined by solving Equations (2) and (3), simultaneously.

$$\dot{Q}_{u,\,col} = A_{col}[G_{abs} - U_{col}(T_{p,col} - T_{amb})] \tag{2}$$

$$T_{p,col} = T_{w,in,col} + \frac{\dot{Q}_{u,\,col}/A_{col}}{U_{col} F_{R,col}}(1 - F_{R,col}) \tag{3}$$

In Equation (3), the heat removal factor ($F_{R,col}$), can subsequently be determined from Equation (4).

$$F_{R,col} = \frac{\dot{m}_{w,in,col} c_{pw,col}}{A_{col} U_{col}} \left[1 - e^{\frac{-A_{col} U_{col} F'_{col}}{\dot{m}_{w,in,col} c_{pw,col}}} \right] \tag{4}$$

where F'_{col} is the collector efficiency factor defined by Equation (5).

$$F'_{col} = \frac{1/U_{col}}{w\left[\frac{1}{U_{col}(2S_\tau F + D_{o,\tau,col})} + \frac{1}{C_B} + \frac{1}{h_{i,\tau,col}\pi D_{i,\tau,col}}\right]} \tag{5}$$

And where F is the fin efficiency given by Equation (6).

$$F = \frac{1}{mL_\tau}\left[\frac{\exp(mL_\tau) - \exp(-mL_\tau)}{\exp(mL_\tau) + \exp(-mL_\tau)}\right] \tag{6}$$

taking the constant m to be defined by Equation (7).

$$m = \sqrt{U_{col}/k_p l_p} \tag{7}$$

Now the overall collector heat loss coefficient (U_{col}) is the summation of the bottom, edge and top heat loss coefficients, where the bottom and edge heat loss coefficient can be calculated from Equations (8) and (9), respectively.

$$U_{bottom} = \frac{k_{ins}}{l_{ins}} \tag{8}$$

$$U_{edge} = U'_{edge}\left(\frac{A_{pr}}{A_{col}}\right) \tag{9}$$

where U' is the edge overall loss coefficient and was assumed to be 0.5.

And the top loss coefficient can be determined from Equation (10) (Agarwal and Larson 1981).

$$U_{top} = \left[\frac{N_{gl,col}}{\frac{Z}{T_{p,col}}\left(\frac{T_{p,col}-T_{amb}}{N_{gl,col}+B}\right)^{0.33}} + \frac{1}{h_{wd}}\right]^{-1} + \frac{\sigma(T_{p,col+}T_{amb})(T_{p,col}^2+T_{amb}^2)}{[\varepsilon_{p,col}+0.5N_{gl,col}(1-\varepsilon_{p,col})]^{-1}+\frac{2N_{gl,col}+B-1}{\varepsilon_{gl,col}}-N_{gl,col}} \tag{10}$$

where $N_{gl,col}$ is the number of glass covers, and B and Z are empirical variables, which are given in Equations (11) and (12).

$$Z = 250[1-0.0044(s-90)] \tag{11}$$

$$B = [1-0.04h_{wd}+0.0005h_{wd}^2][1+0.091N_{gl,col}] \tag{12}$$

Condenser and economiser

As noted previously, the saline water passes through both a condenser and economiser before entering the solar water heater. The condenser was modelled as a gas–liquid single pass shell and tube heat exchanger, as these have been previously used as condensers in HDH desalination systems (Al-Sahali and Ettouney 2008). For a single pass shell and tube heat exchanger, the effectiveness-NTU method can be used to determine the conditions of the outlet fluids, as shown in Equations (13) and (14) (Holman 2010).

$$T_{a,out,cond} = T_{a,in,cond} + \frac{\dot{Q}_{NTU}}{\dot{m}_{a,in,cond}c_{pa,in,cond}} \tag{13}$$

$$T_{w,out,cond} = T_{w,in,cond} - \frac{\dot{Q}_{NTU}}{\dot{m}_{w,in,cond}c_{pw,in,cond}} \tag{14}$$

where the actual heat transfer rate, $\dot{Q}_{NTU}$, is the product of effectiveness and maximum possible energy gain, as presented in Equation (15).

$$\dot{Q}_{NTU} = E\dot{Q}_{max} \tag{15}$$

And where Equation (16) can compute maximum possible energy gained and the effectiveness for a heat exchanger that involves phase change is given in Equation (17).

$$\dot{Q}_{max} = (\dot{m}c_p)_{min}(T_{a,in,cond} - T_{w,in,cond}) \tag{16}$$

taking $(\dot{m}c_p)_{min}$ as the smaller of the heat capacity rate of air $(\dot{m}_a c_{pa})$ and heat capacity ratio of water $(\dot{m}_w c_{pw})$.

$$E_{cond} = 1 - \exp(-NTU) \tag{17}$$

where Equation (18) gives the NTU.

$$NTU = \frac{U_{cond}A_{cond}}{(\dot{m}c_p)_{min}} \tag{18}$$

and, the overall heat transfer coefficient of the condenser can be determined by Equation (19) (Holman 2010).

$$U_{cond} = \frac{1}{\frac{1}{h_a} + \frac{A_{i,\tau}\ln\left[\frac{r_{o,\tau}}{r_{i,\tau}}\right]}{2\pi k_\tau L_\tau} + \frac{A_{i,\tau}}{A_{o,\tau}}\frac{1}{h_w}} \tag{19}$$

For economiser, a liquid–liquid single pass shell and tube heat exchanger is modelled. Similar to the model for the condenser, the effectiveness-NTU method was used to determine the outlet conditions of the fluids from the economiser, as shown in Equation (20), noting that there is no phase change.

$$E_{econ} = 2\left\{1 + c + \sqrt{1+c^2}\,\frac{1 + exp\left[-NTU\sqrt{1+c^2}\right]}{1 - exp\left[-NTU\sqrt{1+c^2}\right]}\right\}^{-1} \tag{20}$$

Where, c is the capacity ratio, as given in Equation (21).

$$c = \frac{(\dot{m}c_p)_{min}}{(\dot{m}c_p)_{max}} \tag{21}$$

And $(\dot{m}c_p)_{max}$ is the larger of the heat capacity rates of air and water.

Humidifier

As shown in Figure 2, the study utilised a novel humidifier, consisting of a series of horizontal trays with a cascading arrangement. As has been mentioned, two main types of interaction occur between the air and the water, counter-current and crossflow. The counter-current interaction flow occurs where water flows along the base and air flows above the water surface. The crossflow interaction occurs when the air passes through the falling water sheet.

In modelling the behaviour of the humidifier, the mass and energy conservation, as well as the correlations of heat and mass transfer, determine the outlet conditions of both air and water streams. For this analysis, steady state conditions were assumed,

hence the conservation of energy is given by Equation (22).

$$\dot{m}_{a,hmd}(\hbar_{a,in,hmd-}\hbar_{a,out,hmd}) = \dot{m}_{w,out,hmd}\hbar_{w,out,hmd} - \dot{m}_{w,in,hmd}\hbar_{w,in,hmd} \tag{22}$$

where the mass flow rate of discharge water from the humidifier can be calculated from Equation (23).

$$\dot{m}_{w,out,hmd} = \dot{m}_{w,in,hmd} - \dot{m}_{ev} \tag{23}$$

And the rate of evaporation can be computed from Equation (24) (Cengel et al. 2002).

$$\dot{m}_{ev} = j\frac{A_{hmd}}{R_v}\left[\frac{P_{sat,f}}{T_f} - \frac{P_{sat,hmd}}{T_{a,hmd}}\right] \tag{24}$$

The mass transfer coefficient (j), associated in Equation (24) can be determined as a function of the Sherwood number as given in Equation (25) (Holman 2010).

$$j = \frac{Sh \times \lambda_{a-w}}{L_{ch}} \tag{25}$$

where the mass diffusion rate for air–water systems ($\lambda_{a\text{-}w}$) can be determined from Equation (26) (Marrero and Mason 1972).

$$\lambda_{a-w} = 1.87 \times 10^{-10}\frac{T^{2.072}}{P} \tag{26}$$

The total rate of heat transfer between air and water is the summation of convective, evaporative and radiative heat transfer. Due to the system operating at moderate temperatures, the radiative heat transfer is neglected. The convective and evaporative heat transfer rates can be determined by Equations (27) and (28), respectively.

$$\dot{Q}_{conv} = h_{conv}A_{hmd}(T_{w,in} - T_{a,in}) \tag{27}$$

$$\dot{Q}_{ev} = \dot{m}_{ev}\hbar_{fg} \tag{28}$$

The coefficient of convective heat transfer (h_{conv}) can be determined as a function of the Nusselt number as given in Equation (29).

$$h_{conv} = \frac{Nu \times k_a}{L_{ch}} \tag{29}$$

Counter-Current interaction

Examining the counter-flow interaction of air and water, the conditions for asymmetric heated rectangular channel were considered as being a suitable representation of the flow. Therefore, the characteristic length in Equations (25) and (29) was taken to be the hydraulic diameter of the duct. For an asymmetric heated rectangular channel and for the aspect ratio of the model, the laminar flow Nusselt number is 3.39 (Cengel 2007). For turbulent conditions, the Nusselt number is given by Equation (30) (Cengel 2007) and the critical Reynolds number for the flow inside the channels is 2300 (Cengel 2007).

$$Nu = 0.023Re^{0.8}Pr^{1/3} \tag{30}$$

As the HDH desalination system operates at a relatively low temperature and atmospheric pressure, this would result in a very small variation of Schmidt and Prandtl number around 0.7. Therefore, the Chilton-Coburn analogy is applicable for the conditions of this study (Cengel 2007), and hence the mass transfer coefficient (j), given in Equation (24) and (25) can also be determined from the analogy as given in Equation (31) (Chilton and Colburn 1934).

$$j = \frac{h_{conv}}{\rho c_p}\left(\frac{Sc}{Pr}\right)^{2/3} \tag{31}$$

Since the heat and mass transfer are analogous, the Sherwood number for laminar flow is identical to the laminar Nusselt number (3.39) and for turbulent flow conditions, Sherwood number can be defined by Equation (32) (Cengel 2007).

$$Sh = 0.023 Re^{0.8} Sc^{1/3} \tag{32}$$

Crossflow interaction

The second flow type experienced in the humidifier is a crossflow, similar to air passing through a waterfall as mentioned previously. In consideration of the crossflow interaction, Enayatollahi et al. (2017b) identified and mapped the existing flow regimes in a crossflow interaction of water, where a ducted airflow crosses through a falling sheet of water. From this they developed a series of correlations for the heat and mass transfer across a range of flow regimes that were used to inform this study. Table 1 shows a summary of the correlations with their range of occurrence.

In a further study (Enayatollahi et al. 2017a) examined the analogy between the heat and mass transfer for the crossflow interaction which led to a modified version of the Chilton-Colburn analogy, as given in Equation (33), which was used here to move between the heat and mass transfer processes occurring in the humidifier.

$$h_t = j\rho_a c_{pa} Le_{ev}^{0.575} \tag{33}$$

Table 1. Experimental correlation of Sherwood and Nusselt numbers for crossflow liquid and gas interaction.

	Flow regime	Criteria	Experimental Correlation
Nusselt Number	Stable	Re < 12500 1.5 < We < 7	$Nu = 3.95 \times 10^{-6}\ Re^{1.88} Pr_{ev}^{0.43}\left(\frac{\dot{m}_w}{\dot{m}_a}\right)^{0.88}$
	Broken	Re > 12500 1.5 < We < 3.3	$Nu = 0.00035\ Pe^{2.9} \mathrm{N}_{ev}^{0.912}$
	Flapping	12500 < Re < 24000 3.3 < We < 7	$Nu = 4.78 \times 10^{-8}\ Re^{2.23} Pr_{ev}^{1.175}$
Sherwood Number	Stable	Re < 12500 1.5 < We < 7	$Sh = 3.95 \times 10^{-6}\ Re^{1.88} Sc_{ev}^{0.43}\left(\frac{\dot{m}_w}{\dot{m}_a}\right)^{0.88}$
	Broken	Re > 12500 1.5 < We < 3.3	$Sh = 0.00035\ Bd^{2.9} \mathrm{N}_{ev}^{0.912}$
	Flapping	12500 < Re < 24000 3.3 < We < 7	$Sh = 4.78 \times 10^{-8}\ Re^{2.23} Sc_{ev}^{1.175}$

Results and discussion

Having outlined the conceptual and parametric modelling of the HDH system, it was decided to examine it via two means. Given the performance of an HDH system is closely tied to the humidifier, the performance of the cascading waterfall humidifier was examined firstly as a stand-alone heat and mass exchanger, then secondly as part of the larger solar HDH desalination system.

A stand-alone cascade humidifier

The performance of a humidifier can be evaluated based on the conditions of the exhaust air and the total amount of evaporation that occurs within it. Therefore, a sensitivity analysis was performed by varying the fluid conditions and operating parameters to determine the temperature of the exhaust air as well as the evaporation rate. Table 2 shows the variables examined, their range of variation, and their nominal values.

As the heat and mass transfer rates are directly related to the mechanism of interaction between the two fluids, changing the air and water mass flow rates transforms the flow regimes. Hence, the effects of both the air and water flow rates needed to be taken into consideration. In particular, increasing the airflow rate at a constant water flow rate can result in the flow regime potentially changing from a 'stable' sheet to a 'flapping' or broken 'sheet' type flow (Enayatollahi et al. 2017b). As shown in Figure 4, increasing the airflow rate under the conditions of a 'stable sheet', where the heat and mass transfer intensities are comparatively weak, initially reduces the temperatures of both exiting air and water streams but increases the total rate of evaporation.

However, further increases to the airflow rate transform the water flow regime to a flapping mode which enhances the heat and mass transfer processes. This results in a higher rate of evaporation and consequently larger temperature drop of the water stream. This is tied to the fact that increasing the airflow rate increases the Reynolds number of air as well as the moisture-carrying capacity of the air stream and thus improves the transfer phenomena. These enhance the total rate of evaporation, and consequently increase the temperature change of the water stream in the humidifier. Conversely, increasing the airflow rate reduces the temperature change of the air stream in the humidifier due to larger mass of air supplied. Once the exhaust air temperature reaches its maximum possible temperature at around 0.015 m^3/s (for a given evaporation area, water and air inlet temperature and water flow rate), increasing the airflow rate reduces the exhaust air temperature due to larger quantities of air supplied.

At lower flow rates of water, increasing the airflow rate, results in transformation of the flow from a stable to broken regime, in which the heat and mass transfer processes are weaker. Therefore, as shown in Figure 5 the evaporation rate as well as the outlet

Table 2. Range of the operating parameters in the cascading humidifier.

Variable	Unit	Range	Nominal Value
Evaporation area (A_{hmd})	(m^2)	0.12–0.75	0.36
Air flow rate ($\dot{V}_a$)	(m^3/s)	0.003–0.032	0.005, 0.03
Water flow rate ($\dot{V}_w$)	(m^3/s)	2×10^{-5}–5×10^{-5}	3.5×10^{-5}, 2.8×10^{-5}
Inlet water temperature ($T_{w,in}$)	($^\circ C$)	25–45	37
Inlet air temperature ($T_{a,in}$)	($^\circ C$)	10–30	20

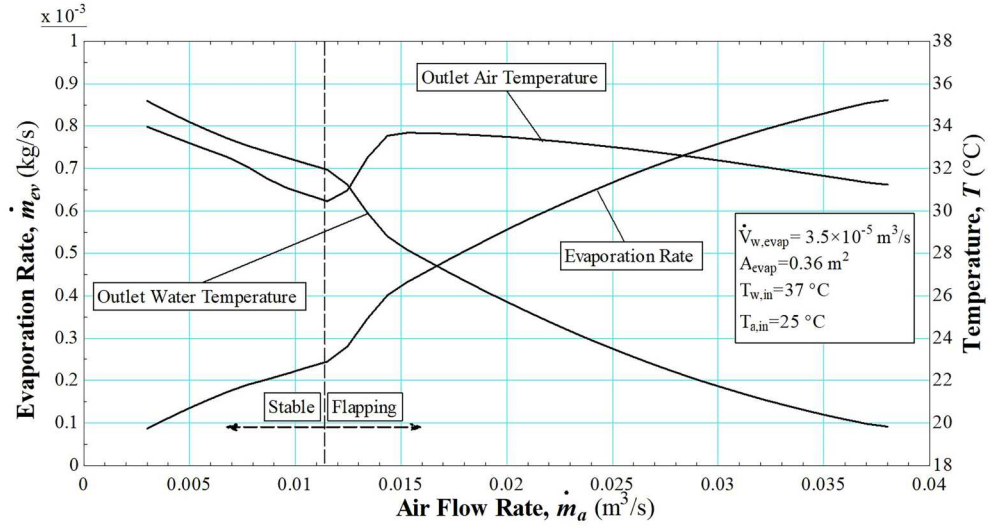

Figure 4. The effect of airflow rate on the evaporation rate and the outlet air and water temperatures from the humidifier at high water flow rate.

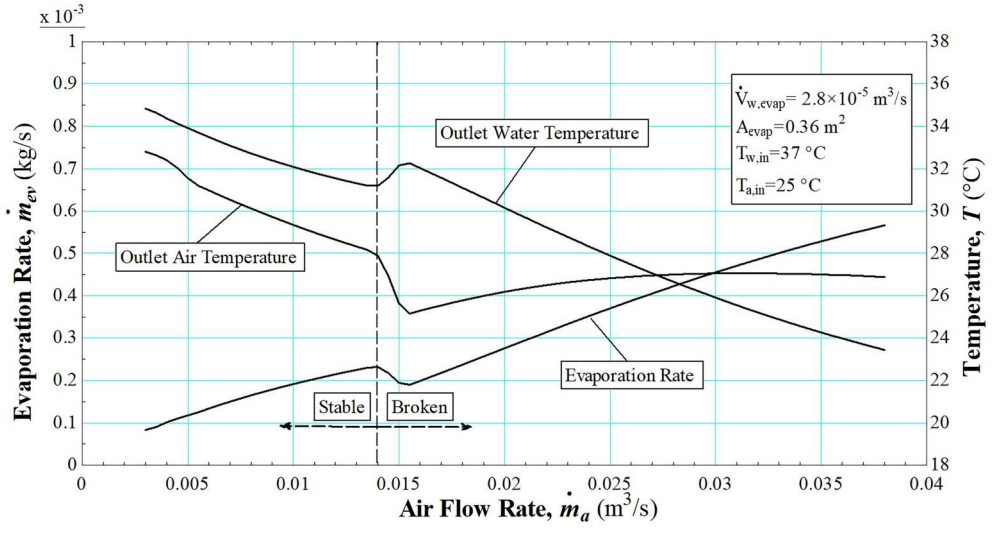

Figure 5. The effect of airflow rate on the evaporation rate and the outlet air and water temperatures from the humidifier at low water flow rate.

temperature of air reduces whereas the discharge water temperature increases with a change of flow regime at an airflow rate of approximately 0.014 m^3/s. However, the broken flow regime occurs at higher flow rates of air where the Reynolds number of the air is larger. Therefore, while the flow regime is broken, increasing the airflow rate enhances the intensities of heat and mass transfer. This initially increases the temperature

of exhaust air, however as illustrated in Figure 5 the temperature of exhaust air drops for flow rates of above approximately 0.03 m^3/s. This can be explained by the fact that the extracted heat from the water stream is transferred to a larger mass of air.

Looking at lower airflow rates, where the crossflow interaction is in a stable regime, as shown in Figure 6, the temperature of the exhaust air, discharge water and evaporation rate increase with increasing the water flow rate. However, the increase is less significant to the discharge water temperature. Increasing the water flow rate while the inlet water temperature is maintained constant and the flow regime is stable (low airflow rates) increases the mass flow ratio, which directly enhances the transfer processes. As a consequence, the temperature of the exhaust air and the evaporation rate increase with increasing the water flow rate, whereas the temperature of the discharge water tends to decrease. Increasing the water flow rate however, reduces the temperature drop across the water stream as a larger mass of water loses heat to the air stream.

Now, considering the effects of water flow rate, it is apparent that increasing the water flow rate, improves the transfer processes by interacting with the air stream on one hand, and on the other hand, by increasing the input heat to the system. Hence, as shown in Figure 7 the temperature of the discharge water decreases whereas the exhaust air temperature increases with increasing the water flow rate. Further increasing the water flow rate transforms the flow to a flapping mode, which enhances the transfer process significantly. Therefore, as illustrated in Figure 7, at a water flow rate of around 2.65×10^{-5} m^3/s, a marked increase can be seen in the outlet air temperature and the evaporation rate.

At higher water flow rates, a larger mass of water loses heat to the airflow, hence, the discharge water temperature increases when the water flow rate is increased beyond approximately 3.1×10^{-5} m^3/s. However, the temperature of inlet water constrains the temperature of the exhaust air, and as a result, the moisture-carrying capacity and the

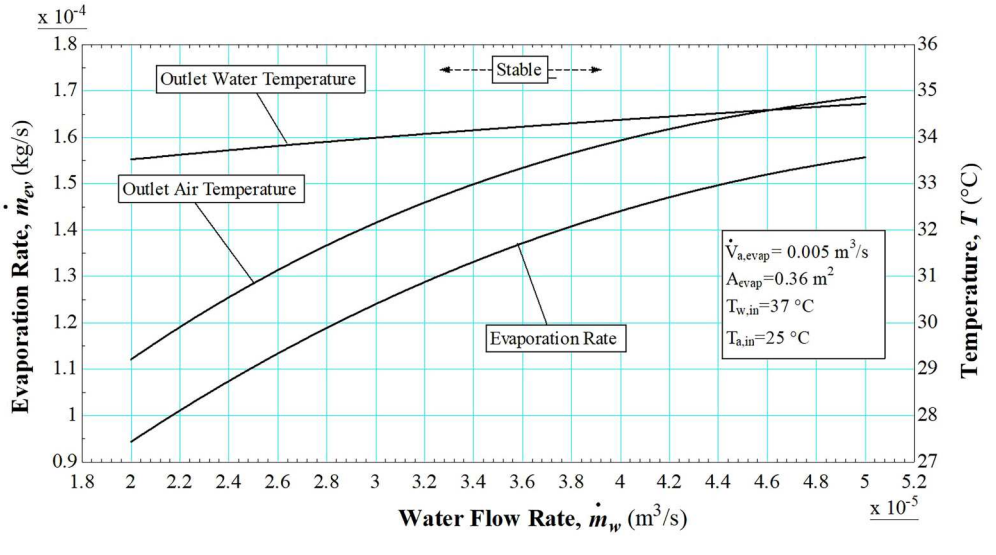

Figure 6. The effect of increasing water flow rate on the evaporation rate and exiting temperature of air and water.

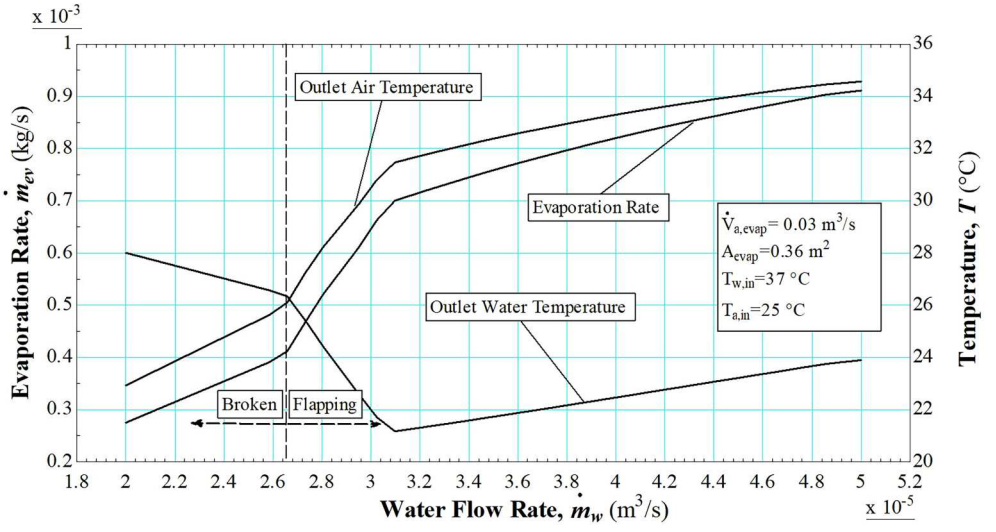

Figure 7. The effect of water flow rate on the outlet temperatures of air and water from the humidifier.

evaporation rate. Hence, the exhaust air temperature and the evaporation rate increase only slightly by increasing the water flow rate above 3.1×10^{-5} m^3/s.

Finally, as shown in Figure 8 enlarging the area of the humidifier increases the evaporation rate and the temperature of the exiting moist air, while decreasing the temperature of the discharge water. The area of evaporation can be increased by adding additional trays in the humidifier, which also increases the number of crossflow contacts in the system. In this respect, the temperature of the inlet water constrains the temperature and moisture-carrying capacity of the air and as a result, the evaporation rate.

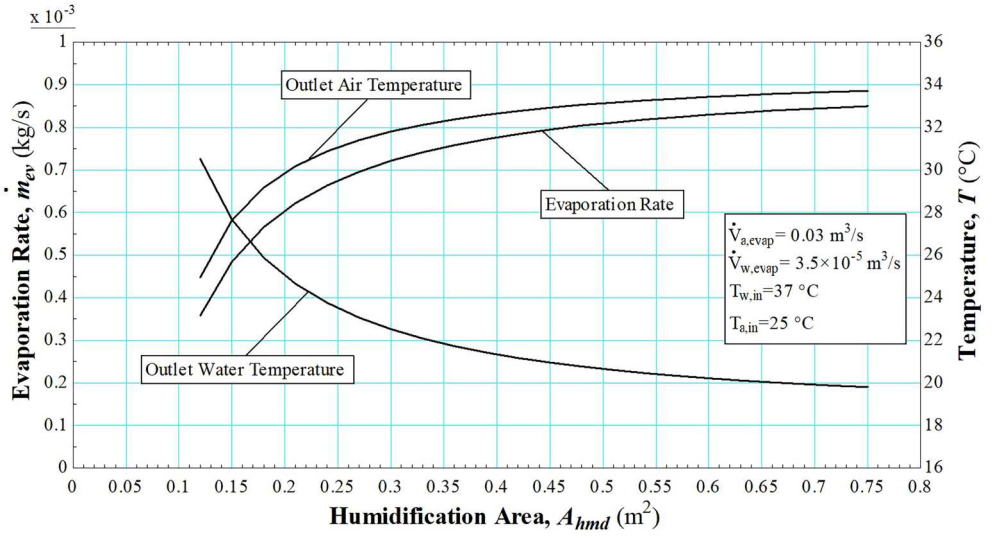

Figure 8. Effect of evaporation area on the rate of evaporation and the temperature of exiting air and water.

However, as shown in Figure 8, increasing the area of evaporation beyond 0.45m^2 does not provide a significant increase in the evaporation rate and hence, the outlet temperatures of air and water change only slightly.

On the whole, the model of the humidifier shows an effective transfer phenomenon in the bioinspired cascading configuration, which justifies its application in the HDH desalination systems.

Solar HDH desalination system with cascading humidifier

In this section, the performance of the novel cascading humidifier in the solar desalination system, shown in Figure 1, is examined. The design parameters for the cascading humidifier and the other parts of the system are given in Table 3.

In order to be able to design and develop an HDH desalination system for a particular location, the sensitivity of the climatic and operational parameters on the rate of production needs to be evaluated. Table 4 shows the range and the nominal values of the examined parameters.

As shown in Figure 9, increasing the radiation received by the solar water heater increases the evaporation in the humidifier. This is because it puts extra energy into the water stream, which consequently increases the production of the system.

As illustrated in Figure 10, increasing the airflow rate initially increases the system production, but above 0.8×10^{-2} m^3/s this begins to decrease. However, further increasing the airflow rate above 1.2×10^{-2} m^3/s increases the yield of the system as a result of a change in the flow regime of the water sheet. Increasing the airflow rate, increases the moisture carrying capacity of the air stream. Additionally, the formation of the 'flapping' regime, due to increased airflow, develops a turbulent flow, and thus significantly enhances the intensities of heat and mass transfer and consequently the potable water production.

Now, looking at the effects of increasing the water flow rate, it can be concluded that; increasing the water flow rate enhances the cooling process in the dehumidifier, but weakens the preheating and heating processes in the economiser and the solar water collector. Taking both effects into consideration, increasing the water flow rate, increases the production of the system very gradually. Further, increases in the flow rate of water

Table 3. Design parameters of the HDH desalination with cascading humidifier.

Water Collector		Humidifier		Condenser		Economiser	
$N_{g,col}$	2 [-]	A_{hmd}	0.49 [m^2]	$N_{\tau,cond}$	20 [-]	$N_{\tau,econ}$	20 [-]
$N_{\tau,col}$	20 [-]	$L_{Tr,hmd}$	0.35 [m]	$N_{bf,cond}$	19 [-]	$N_{bf,econ}$	19 [-]
$D_{o,\tau,col}$	0.0127 [m]	$W_{Tr,hmd}$	0.1 [m]	$D_{o,\tau,cond}$	0.0127 [m]	$D_{o,\tau,econ}$	0.0127 [m]
$D_{i,\tau,col}$	0.01181 [m]	$H_{ch,hmd}$	0.05 [m]	$D_{i,\tau,cond}$	0.01181 [m]	$D_{i,\tau,econ}$	0.01181 [m]

Table 4. Range of the independent variables for sensitivity analysis.

Variable	Unit	Range	Nominal Value
Evaporation area (A_{hmd})	(m^2)	0.14–0.49	0.49
Air flow rate ($\dot{V}_a$)	(m^3/s)	0.003–0.03	0.025
Water flow rate ($\dot{V}_w$)	(m^3/s)	2×10^{-5}–5×10^{-5}	3.3×10^{-5}
Total Radiation (G_t)	(W/m^2)	300–1300	1000

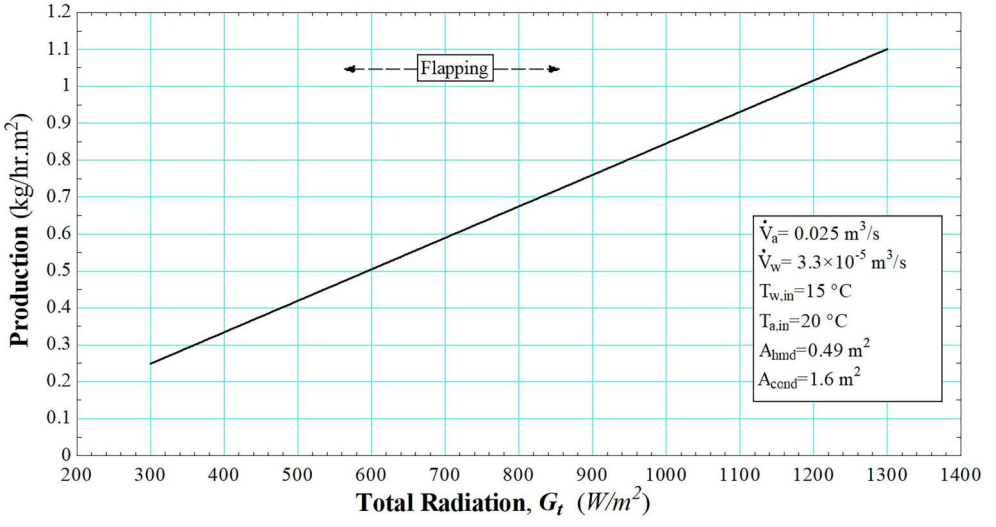

Figure 9. Variation of production versus radiation.

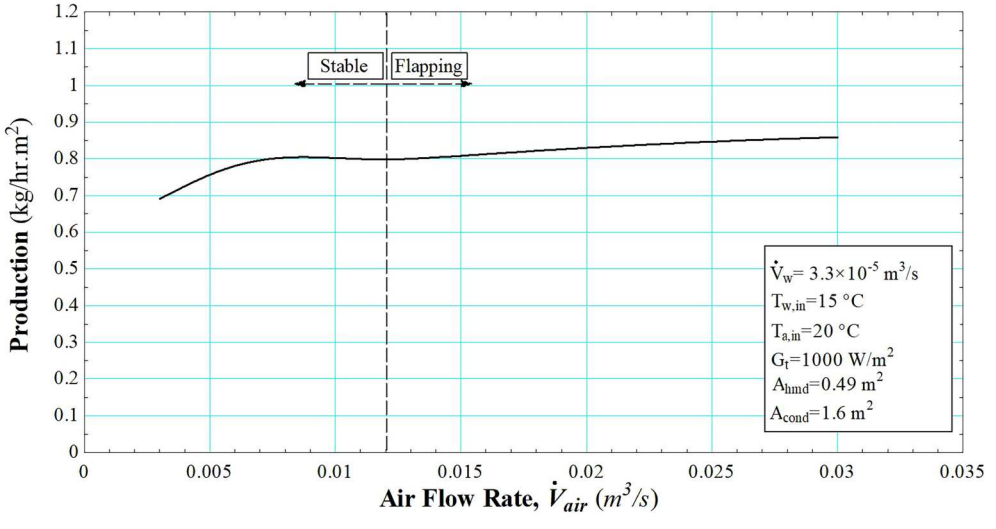

Figure 10. Variation of production versus airflow rate.

transform the flow regime from broken to flapping sheets, which enhances the transfer phenomena in the humidifier. This, as discussed previously, increases the evaporation rate but at the same time reduces the temperature of the discharge water from the humidifier. Therefore, as shown in Figure 11, the effect of increasing the water flow rate on the rate of production was found to be very small.

Finally, the variation of potable production versus the number of cascade trays in the humidifier is shown in Figure 12. Adding more trays in the humidifier, increases the area of evaporation and the number of crossflow interactions, which increase the total yield of

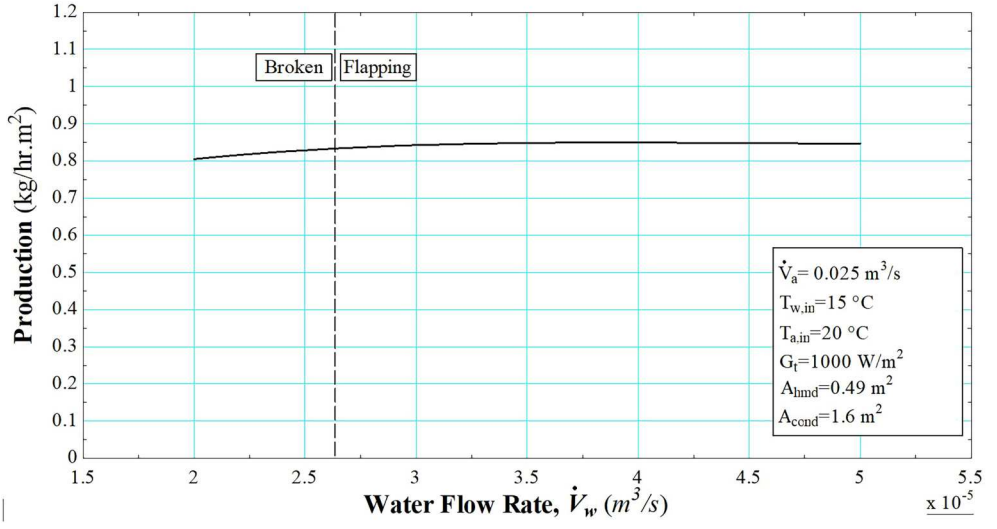

Figure 11. Variation of production versus water flow rate.

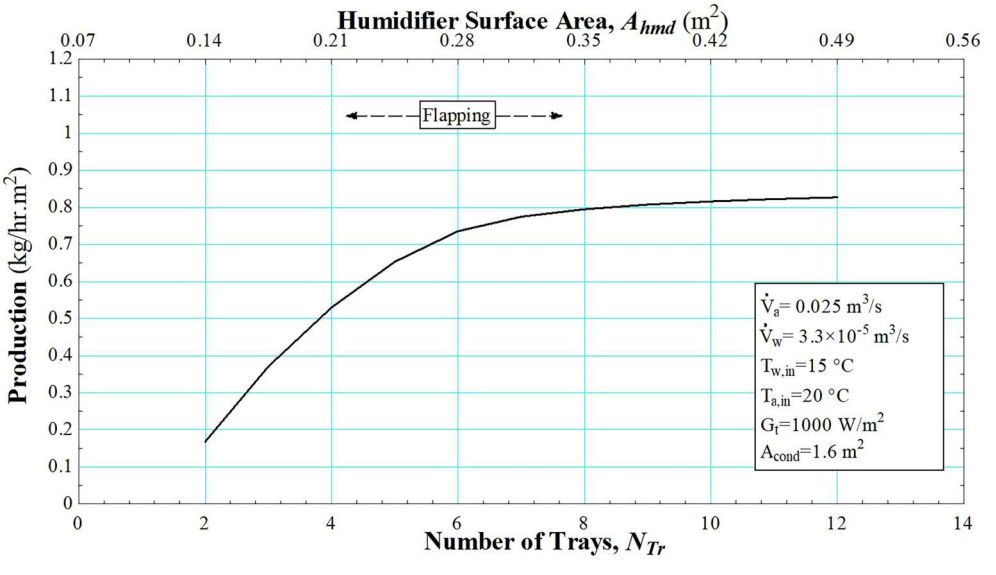

Figure 12. Variation of production versus the number of trays and surface area in the humidifier.

the system. However, the temperature of the exhaust air from the humidifier and consequently the rate of evaporation is limited by the inlet water temperature to the humidifier. Therefore, once the evaporation rate in the humidifier is maximized, increasing the number of trays (or evaporation area) does not increase production unless additional energy is added to the system.

As mentioned earlier, two interaction mechanisms exist in the cascading humidifier, a crossflow, that is due to air crossing through the falling water sheets, and a counterflow

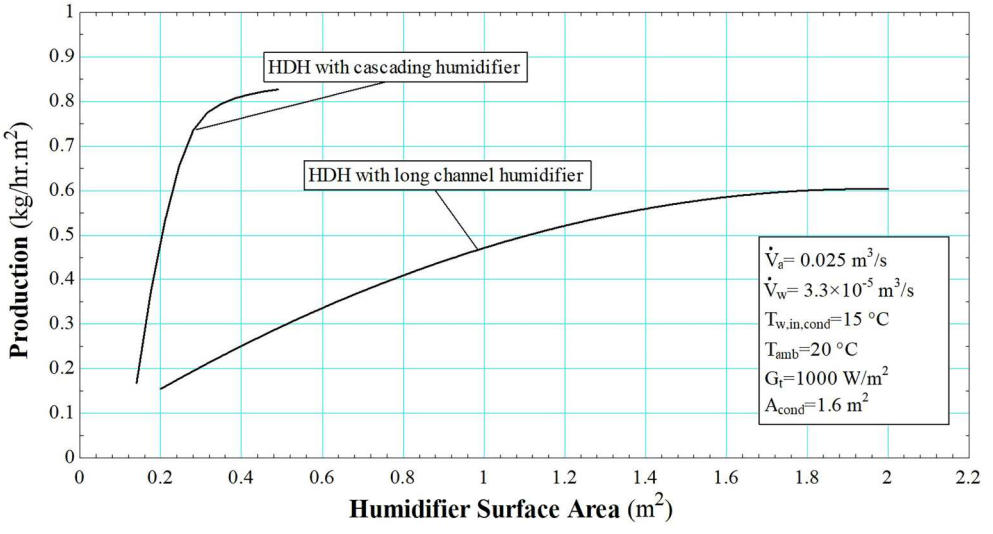

Figure 13. Comparing the performance of the proposed cascading humidifier with a simple rectangular duct humidifier.

flow configuration that is simply the flow of air and water in a horizontal rectangular duct in opposite directions. To be able to compare the performance of the proposed cascading humidifier, a simple humidifier, consist of a long square duct with water flowing at the bottom of the channel and air flowing over water in a counterflow configuration was mathematically modelled. Figure 13 shows the comparison of the performance of the proposed cascading humidifier, and the simple square duct humidifier. Under the same operational condition, the application of the cascade humidifier can increase the production by nearly 40% while reducing the required area by 75%.

Conclusions

This work examined the conceptual design of a solar HDH desalination system with a view to application in remote and decentralized locations. In this regard, a novel bio-inspired cascading humidifier was proposed. The sensitivity of fresh water production in the system was parametrically evaluated against the climatic conditions and operational parameters. In consideration of the performance of the cascading humidifier, it was found that the moist air temperature depends mostly on the inlet water temperature, but the temperature of the exiting brine is influenced by both air and water inlet temperatures. The effect of varying air and water flow rates was found to be significant as they influence the flow regimes in the crossflow interactions. In particular, when examining the entire HDH system, it was found that increasing the water flow rate in the system lowers the fresh water production whereas increasing the air flow rate tends to increase the production rate.

Disclosure statement

No potential conflict of interest was reported by the author(s).

ORCID

Timothy Anderson http://orcid.org/0000-0002-0972-5206

References

Abdel Dayem AM, AlZahrani A. 2022. Psychometric study and performance investigation of an efficient evaporative solar HDH water desalination system. Sustainable Energy Technologies and Assessments. 52:102030. doi:10.1016/j.seta.2022.102030.

Abokersh MH, El-Morsi M, Sharaf O, Abdelrahman W. 2017. On-demand operation of a compact solar water heater based on U-pipe evacuated tube solar collector combined with phase change material. Solar Energy. 155:1130–1147. doi:10.1016/j.solener.2017.07.008.

Abu El-Maaty AE, Awad MM, Sultan GI, Hamed AM. 2023. Innovative approaches to solar desalination: a comprehensive review of recent research. Energies. 16(9):3957. doi:10.3390/en16093957.

Agarwal VK, Larson DC. 1981. Calculation of the top loss coefficient of a flat-plate collector. Solar Energy. 27(1):69–71. doi:10.1016/0038-092X(81)90022-0.

Al-Enezi G, Ettouney H, Fawzy N. 2006. Low temperature humidification dehumidification desalination process. Energy Conversion and Management. 47(4):470–484. doi:10.1016/j.enconman.2005.04.010.

Al-Hallaj S, Farid MM, Tamimi AR. 1998. Solar desalination with a humidification-dehumidification cycle: performance of the unit. Desalination. 120(3):273–280. doi:10.1016/S0011-9164(98)00224-0.

Al-Juwayhel F, El-Dessouky H, Ettouney H. 1997. Analysis of single-effect evaporator desalination systems combined with vapor compression heat pumps. Desalination. 114(3):253–275. doi:10.1016/S0011-9164(98)00017-4.

Al-Sahali M, Ettouney HM. 2008. Humidification dehumidification desalination process: design and performance evaluation. Chemical Engineering Journal. 143(1):257–264. doi:10.1016/j.cej.2008.04.030.

Al-Sulaiman FA, Zubair MI, Atif M, Gandhidasan P, Al-Dini SA, Antar MA. 2015. Humidification dehumidification desalination system using parabolic trough solar air collector. Applied Thermal Engineering. 75:809–816. doi:10.1016/j.applthermaleng.2014.10.072.

Cengel YA. 2007. Heat and mass transfer, 3rd ed. New York: McGraw-Hill.

Cengel YA, Boles MA, Kanoğlu M. 2002. Thermodynamics: an engineering approach. New York: McGraw-Hill.

Chilton TH, Colburn AP. 1934. Mass transfer (absorption) coefficients prediction from data on heat transfer and fluid friction. Industrial & Engineering Chemistry. 26(11):1183–1187. doi:10.1021/ie50299a012.

Duffie JA, Beckman WA. 1980. Solar engineering of thermal processes. New York: Wiley.

Elminshawy NAS, Siddiqui FR, Sultan GI. 2015. Development of a desalination system driven by solar energy and low grade waste heat. Energy Conversion and Management. 103:28–35. doi:10.1016/j.enconman.2015.06.035.

Enayatollahi R, Nates RJ, Anderson T. 2017a. The analogy between heat and mass transfer in low temperature crossflow evaporation. International Communications in Heat and Mass Transfer. 86:126–130. doi:10.1016/j.icheatmasstransfer.2017.06.002.

Enayatollahi R, Nates RJ, Anderson T. 2017b. Characterising the heat and mass transfer coefficients for a crossflow interaction of air and water. International Journal of Heat and Mass Transfer. 111:94–104. doi:10.1016/j.ijheatmasstransfer.2017.03.098.

Fouda A, Nada SA, Elattar HF, Rubaiee S, Al-Zahrani A. 2018. Performance analysis of proposed solar HDH water desalination systems for hot and humid climate cities. Applied Thermal Engineering. 144:81–95. doi:10.1016/j.applthermaleng.2018.08.037.

Gill RS, Singh S, Singh PP. 2012. Low cost solar air heater. Energy Conversion and Management. 57:131–142. doi:10.1016/j.enconman.2011.12.019.

Giwa A, Akther N, Housani AA, Haris S, Hasan SW. 2016. Recent advances in humidification dehumidification (HDH) desalination processes: improved designs and productivity. Renewable and Sustainable Energy Reviews. 57:929–944. doi:10.1016/j.rser.2015.12.108.

Holman J. 2010. Heat transfer, 10th ed. Boston.: McGraw-Hill Higher Education.

Hussain Soomro S, Santosh R, Bak C-U, Yoo C-H, Kim W-S, Kim Y-D. 2022. Effect of humidifier characteristics on performance of a small-scale humidification-dehumidification desalination system. Applied Thermal Engineering. 210:118400. doi:10.1016/j.applthermaleng.2022.118400.

Klein SA. 2016. Engineering equation solver. Academic professional. V10.103 ed. Madison, WI: F-Chart Software.

Lawal DU, Qasem NAA. 2020. Humidification-dehumidification desalination systems driven by thermal-based renewable and low-grade energy sources: a critical review. Renewable and Sustainable Energy Reviews. 125:109817. doi:10.1016/j.rser.2020.109817.

Luberti M, Capocelli M. 2023. Enhanced Humidification–Dehumidification (HDH) systems for sustainable water desalination. Energies. 16(17):6352. doi:10.3390/en16176352.

Luo T, Young R, Reig P. 2015. Aqueduct projected water stress country rankings. Technical Note. 16.

Marrero TR, Mason EA. 1972. Gaseous diffusion coefficients. Journal of Physical and Chemical Reference Data. 1(1):3–118. doi:10.1063/1.3253094.

Morrison GL, Budihardjo I, Behnia M. 2004. Water-in-glass evacuated tube solar water heaters. Solar Energy. 76(1-3):135–140. doi:10.1016/j.solener.2003.07.024.

Narayan GP, Sharqawy MH, Summers EK, Lienhard JH, Zubair SM, Antar MA. 2010. The potential of solar-driven humidification–dehumidification desalination for small-scale decentralized water production. Renewable and Sustainable Energy Reviews. 14(4):1187–1201. doi:10.1016/j.rser.2009.11.014.

Nowzari R, Saygin H, Aldabbagh LBY. 2021. Evaluating the performance of a modified solar air heater with pierced cover and packed mesh layers. Journal of Solar Energy Engineering. 143 (1). doi:10.1115/1.4047528.

Qtaishat MR, Banat F. 2013. Desalination by solar powered membrane distillation systems. Desalination. 308:186–197. doi:10.1016/j.desal.2012.01.021.

Sabiha MA, Saidur R, Mekhilef S, Mahian O. 2015. Progress and latest developments of evacuated tube solar collectors. Renewable and Sustainable Energy Reviews. 51:1038–1054. doi:10.1016/j.rser.2015.07.016.

Shaikh JS, Ismail S. 2022. A review on recent technological advancements in humidification dehumidification (HDH) desalination. Journal of Environmental Chemical Engineering. 10 (6):108890. doi:10.1016/j.jece.2022.108890.

Shamet O, Lawal DU, AlHariri AH, Antar M. 2023. Performance of different HDH desalination units powered by diesel engine generator waste heat. Process Safety and Environmental Protection. 179:651–666. doi:10.1016/j.psep.2023.09.046.

Srithar K, Rajaseenivasan T. 2018. Recent fresh water augmentation techniques in solar still and HDH desalination – A review. Renewable and Sustainable Energy Reviews. 82:629–644. doi:10.1016/j.rser.2017.09.056.

Tan X, Saha P, Klausner J, Abbasi B, Benard A. 2023. Modeling and experimental validation of direct contact crossflow packed beds condenser used in HDH desalination systems. Desalination. 548:116297. doi:10.1016/j.desal.2022.116297.

Yuan G, Zhang H. 2007. Mathematical modeling of a closed circulation solar desalination unit with humidification–dehumidification. Desalination. 205(1):156–162. doi:10.1016/j.desal.2006.03.550.

Zamen M, Soufari SM, Vahdat SA, Amidpour M, Zeinali MA, Izanloo H, Aghababaie H. 2014. Experimental investigation of a two-stage solar humidification–dehumidification desalination process. Desalination. 332(1):1–6. doi:10.1016/j.desal.2013.10.018.

Zarei T, Miroliaei MR. 2022. Performance evaluation of an HDH desalination system using direct contact packed towers: experimental and mathematical modeling study. Water Reuse. 12(1):92–110.